

Direct visualization of the transverse photoemission position within molecules via strong-field photoelectron holography

Jia Tan ^{1,*}, Qinghua Ke ², Dian Wang,³ Xiang Hao,¹ Jialing Xie,¹ Guo Yu,¹ Xue Xu,¹ and Quanying Wu¹

¹*Jiangsu Key Laboratory of Micro and Nano Heat Fluid Flow Technology and Energy Application, School of Physical Science and Technology, Suzhou University of Science and Technology, Suzhou 215009, China*

²*School of Physics and Wuhan National Laboratory for Optoelectronics, Huazhong University of Science and Technology, Wuhan 430074, China*

³*School of Mathematics and Physics, Hubei Polytechnic University, Huangshi 435003, China*



(Received 26 March 2023; revised 23 May 2023; accepted 25 July 2023; published 7 August 2023)

Laser-induced tunneling ionization triggers a broad class of strong-field phenomena in the attosecond community. The understanding and application of these ultrafast phenomena require accurate knowledge of the position information for the tunneling electron wave packet (EWP). Here, with strong-field photoelectron holography, we theoretically demonstrate a scheme to retrieve the position of the EWP emitted from molecules in the direction perpendicular to the tunnel. In our scheme, the photoelectron momentum distributions from strong-field tunneling ionization are obtained by solving the time-dependent Schrödinger equation. When the molecule is aligned with a nonzero angle to the linearly polarized laser field, a distinct shift of the holographic pattern in the photoelectron momentum distribution is observed. With the quantum-orbit model, we demonstrate that the shift of the holographic pattern is caused by a nonzero initial transverse position of the EWP immediately after tunneling. By tracing their exact correspondence and examining the shift of the holographic pattern, the transverse emission position of the tunnel-ionized EWP is probed accurately. Furthermore, we demonstrate that the complex Coulomb interaction can be safely canceled in our scheme by performing the scheme for both of the model molecules with the short-range and Coulomb potentials. The validity and accuracy of our scheme are confirmed by its application to different molecules, alignments, and laser parameters.

DOI: [10.1103/PhysRevA.108.023110](https://doi.org/10.1103/PhysRevA.108.023110)

I. INTRODUCTION

Laser-induced atom or molecule tunneling ionization is one of the most fundamental light-matter interaction processes and it initiates a broad range of ultrafast phenomena in the science community, such as high harmonic generation [1], high-order above-threshold ionization [2], and enhanced multiple ionization [3–5]. Understanding these ultrafast phenomena and exploring their application are the fundamental tasks of attosecond physics; therein accurate dynamic information of the tunnel-ionized electron wave packet (EWP) is essential. During the past years, much effort has been paid to exploring the dynamics of the EWP from strong-field tunneling ionization of atoms or molecules, such as the time when the electron exits the tunneling barrier [6–8], the time needed for an electron to tunnel through the potential barrier [9–13], the phase accumulated when a electron tunnels through the potential barrier [14–16], and the initial momentum distribution of the EWP at the tunnel exit [17]. Recently, another important issue, the emission position of the EWP in tunneling ionization, has aroused wide concern.

The emission position of the EWP is involved in various trajectory-based models, from which the EWP is tunneling ionized through the potential barrier, and then accelerated by the oscillating electric field of the laser pulse [18]. In previous

studies, many physical processes triggered by tunneling ionization in laser-atom or molecule interactions were explained with the trajectory-based concept [19–25]. In these applications, the accurate knowledge of the emission position for the tunneling EWP is required. Generally, the position component longitudinal to the direction of the instantaneous tunneling is estimated by $-I_p/E(t)$, where I_p is the ionization potential of the atom or molecule and $E(t)$ is the instantaneous laser field. Recently, the rapidly developing attosecond technique facilitated the more accurate measurement of the longitudinal component [26]. For the transverse emission position of the EWP, the value is always zero in atoms since the tunnel ionization is limited along the direction of the instantaneous electric field, while in molecules, it is affected by the molecular orbital and alignment [27].

A nonzero displacement of the EWP in position space corresponds to an additional phase of the continuous electron in momentum space. In previous studies, it was reported that the phase structure of the EWP immediately after tunneling could be extracted from the holographic interference in photoelectron momentum distributions (PEMDs) [28]. In their study, with the quantum-trajectory Monte Carlo method, the asymmetry of holographic interference was reproduced by artificially adding an initial phase to the tunneling EWP. Recently, another basic insight was offered. It was proposed that the transverse emission position of the tunneling EWP can be directly probed by analyzing the phase distribution of the holographic pattern [29]. In this scheme, gaining the

*Corresponding author: jiatansust@163.com

linear phase distribution of the hologram was the key step. In strong-field tunneling ionization, the holographic pattern is originated from the interference of the EWP reaching to the detector directly after tunneling and that undergoing a near-forward rescattering with the parent ion [30]. Because of the near-forward rescattering, the interference signal is usually weak for the momentum region away from the field-polarization axis, and in experiments, the hologram in that momentum region is not even clear due to the laser focal volume effect [31,32]. Additionally, the carpet-like interference between the direct electrons dominates the spectrum away from the field-polarization axis, which can seriously influence the extraction of the linear phase distribution from the hologram [33]. Therefore, it is still difficult to obtain the transverse emission position of the tunneling EWP from the hologram.

Strong-field photoelectron holography (SFPH) is considered as a powerful tool to probe the structural and temporal properties of atomic or molecular systems with angstrom and attosecond precision in which the structure and ultrafast dynamics of atoms or molecules are encoded in the hologram through the delivery of EWPs. In the past years, SFPH has been widely reported [34–38]. Recently, it was demonstrated that the phase of the scattering amplitude for atoms or molecules (structure information) [39], the dynamics of the ultrafast charge migration in molecules [40], and the ionization time information of the tunneling process can be retrieved from the SFPH structure accurately [41–43]. Here, we apply SFPH to survey the property of the EWP in strong-field tunneling ionization.

In this work, we demonstrate a retrieval of the transverse position for the EWP emitted from the molecule in tunneling ionization with SFPH. By solving the time-dependent Schrödinger equation, we show that the hologram in the PEMD exhibits a distinct shift along the direction perpendicular to the laser polarization, when the molecule is aligned with a nonzero angle to the linear laser field. With the quantum-orbit model, we demonstrate that the shift of holographic pattern corresponds to a nonzero transverse emission position of the tunneling EWP. By tracing their exact correspondence and examining the shift of holographic interference near the field-polarization axis, we show the transverse emission position of the tunnel-ionized EWP is retrieved precisely. In strong-field tunneling ionization, the effect of the long-range Coulomb potential on the EWP is complex [44–46]. Here, by performing our scheme for both of the model molecules with short-range and Coulomb potentials, we demonstrate that its influence on the shift of holographic pattern can be safely canceled, and thus the retrieval processes are greatly simplified. Additionally, the validity and accuracy of our scheme are confirmed by applying it to different molecules, alignments, and laser parameters.

II. THEORETICAL METHODS

A. Numerically solving 2D-TDSE

In the work, PEMDs for strong-field tunneling ionization of molecules are obtained by solving the two-dimensional time-dependent Schrödinger equation (2D-TDSE) of (atomic

TABLE I. The parameters of the one-electron soft-core potential for the 2D mimic H_2^+ and N_2

	H_2^+		N_2	
	H	H	N	N
a_α	0.83	0.83	1.2	1.2
σ_α^2	∞	∞	0.7	0.7
Z_α^0	1	1	7	7
Z_α^∞	1	1	0.5	0.5
R_0	4		2	

units are used throughout)

$$i \frac{\partial \Psi(\mathbf{r}, t)}{\partial t} = H(\mathbf{r}, t) \Psi(\mathbf{r}, t), \quad (1)$$

where $\Psi(\mathbf{r}, t)$ is the electron wave function and $\mathbf{r} = (x, y)$ indicates its position in the polarization plane of the laser field. In length gauge, the Hamiltonian $H(\mathbf{r}, t)$ is written as

$$H(\mathbf{r}, t) = -\frac{1}{2} \nabla^2 + V(\mathbf{r}) + \mathbf{r} \cdot \mathbf{E}(t), \quad (2)$$

with the one-electron soft-core potential of $V(\mathbf{r}) = \sum_{\alpha}^{N=2} -Z_\alpha(\mathbf{r}_\alpha) / \sqrt{|\mathbf{r}_\alpha|^2 + a_\alpha^2}$. Here, a_α is the soft-core parameter and $\mathbf{r}_\alpha = \mathbf{r} - \mathbf{R}_\alpha/2$. α labels the nuclei at the position of $\mathbf{R}_\alpha/2$ and $Z_\alpha = Z_\alpha^0 + (Z_\alpha^0 - Z_\alpha^\infty) \exp(-|\mathbf{r}_\alpha|^2 / \sigma_\alpha^2)$ is the position-dependent effective charge, where σ_α characterizes the decrease of the effective charge with $|\mathbf{r}_\alpha|$ [47]. In our calculation, the parameters of Table I are adopted to produce the ground state with the same angular momentum as N_2 and H_2^+ . The laser field is linearly polarized along the \hat{x} axis, and the electric field of which is written as

$$\mathbf{E}(t) = -f(t) E_0 \cos(\omega t) \hat{x}, \quad (3)$$

where E_0 is the amplitude and ω is the angular frequency. $f(t)$ is the envelope function of the laser field, which has the trapezoidal form, ramping on and off over one optical cycle with a plateau of three optical cycles. The wavelength of the laser field is 1000 nm and the intensity is $2.5 \times 10^{14} \text{ W/cm}^2$.

To solve the 2D-TDSE of Eq. (1), we prepare the initial wave function by the imaginary time propagation of the field-free system [48]. The time-dependent wave function $\Psi(\mathbf{r}, t)$ is then propagated using the split-operator method on a Cartesian grid $\zeta \times \zeta$ with $\zeta = 700$ a.u. [49]. The time step is fixed at $\Delta t = 0.06$ a.u. and the spatial discretization is $\Delta x = \Delta y = 0.2$ a.u.. After the end of the laser pulse, the wave function is further propagated for four additional optical cycles of the laser pulse to make sure the ionized part moves away from the core. The PEMD is eventually calculated by Fourier transform of the ionized wave function, which is obtained by filtering out the bound part of the total wave function with a $\cos^{1/2}$ -mask function [50,51].

B. Quantum-orbit model

Our scheme is based on the holographic structure in PEMDs, which is determined by the phase difference between the near-forward rescattering and direct EWPs, i.e.,

$$M^2 = |M_d + M_r|^2 = |M_d|^2 + |M_r|^2 + 2|M_d||M_r| \cos(\Delta\Phi). \quad (4)$$

Here, M_d and M_r are the transition amplitudes of the direct and near-forward rescattering EWPs, respectively, and $\Delta\Phi$ denotes their phase difference. In previous studies [39], it was reported that $\Delta\Phi$ has the form of

$$\Delta\Phi = \Delta\Phi_F + \alpha, \quad (5)$$

where $\Delta\Phi_F$ accounts for the phase difference accumulated during the propagation of direct and near-forward rescattering electrons in the laser field, and α indicates the phase induced by the Coulomb interaction of the rescattering electrons with the parent ion.

Following the quantum-orbit (QO) model, the phase difference $\Delta\Phi_F$ can be obtained with the saddle-point method, which provides us the quantum orbits to analyze the holographic interference in PEMDs [52–63]. Thus, $\Delta\Phi_F$ is given by

$$\Delta\Phi_F = S_r - S_d = \int_{t_0^d}^{t_r} \frac{[\mathbf{p} + \mathbf{A}(t)]^2}{2} dt - \int_{t_0^r}^{t_r} \frac{[\mathbf{k} + \mathbf{A}(t)]^2}{2} dt + I_p(t_0^r - t_0^d) + [\mathbf{k} + \mathbf{A}(t_0^r) - \mathbf{p} - \mathbf{A}(t_0^d)] \cdot \mathbf{R}, \quad (6)$$

where $S_d = -\{\int_{t_0^d}^{T_f} [\mathbf{p} + \mathbf{A}(t)]^2/2dt - \int_0^{t_0^d} I_p dt\} + [\mathbf{p} + \mathbf{A}(t_0^d)] \cdot \mathbf{R}$ and $S_r = -\{\int_{t_0^r}^{T_f} [\mathbf{k} + \mathbf{A}(t)]^2/2dt + \int_0^{t_0^r} [\mathbf{k} + \mathbf{A}(t)]^2/2dt - \int_0^{t_0^r} I_p dt\} + [\mathbf{k} + \mathbf{A}(t_0^r)] \cdot \mathbf{R}$ represent the phases of the transition amplitudes for the direct and near-forward rescattering electrons. In these phases, \mathbf{p} is the final momentum of the electron and \mathbf{k} is the intermediate canonical momentum of the electron before rescattering. t_0^d and t_r are the ionization and rescattering times of the rescattering electron. t_0^d is the ionization time of the direct electron. I_p indicates the ionization potential of the molecule and $\mathbf{R} = (x_0, y_0)$ shows the coordinate of the electron immediately after tunneling in which x_0 and y_0 denote the longitudinal (along the polarization direction of the laser field) and transverse displacements, respectively. $\mathbf{A}(t) = -\int_{-\infty}^t \mathbf{E}(t') dt'$ is the vector potential of the laser pulse, and T_f denotes the pulse turn-off time.

For the linearly polarized laser field that we employed, $\Delta\Phi_F$ could be further divided two parts:

$$\Delta\Phi_{F_x} = \int_{t_0^d}^{t_r} \frac{[p_x + A(t)]^2}{2} dt - \int_{t_0^r}^{t_r} \frac{[k_x + A(t)]^2}{2} dt + [k_x + A(t_0^r) - p_x - A(t_0^d)]x_0 + I_p(t_0^r - t_0^d) \quad (7)$$

and

$$\Delta\Phi_{F_y} = \int_{t_0^d}^{t_r} \frac{p_y^2}{2} dt - \int_{t_0^r}^{t_r} \frac{k_y^2}{2} dt + (k_y - p_y)y_0. \quad (8)$$

In Eqs. (7) and (8), p_x and p_y are the final parallel and transverse (perpendicular to the laser polarization direction) momenta of the electron. k_x and k_y are the parallel and transverse components of \mathbf{k} . For the direct electron, the ionization time t_0^d can be obtained from the saddle-point equation $[\partial(S_d)/\partial t_0^d = 0]$ of

$$\frac{1}{2}[p_x + A(t_0^d)]^2 + \frac{1}{2}p_y^2 + I_p - x_0 E(t_0^d) = 0. \quad (9)$$

For the rescattering electron, the ionization and rescattering times of t_0^r and t_r are determined by the saddle-point equations $[\partial(S_r)/\partial t_0^r = 0, \partial(S_r)/\partial t_r = 0$ and $\partial(S_r)/\partial \mathbf{k} = 0]$ of

$$\frac{1}{2}[k_x + A(t_0^r)]^2 + \frac{1}{2}k_y^2 + I_p - x_0 E(t_0^r) = 0, \quad (10)$$

$$\frac{1}{2}[k_x + A(t_r)]^2 + \frac{1}{2}k_y^2 = \frac{1}{2}[p_x + A(t_r)]^2 + \frac{1}{2}p_y^2, \quad (11)$$

$$\int_{t_0^r}^{t_r} [k_x + A(t)] dt = x_0, \quad (12)$$

$$\int_{t_0^r}^{t_r} k_y dt = y_0.$$

Physically, Eq. (9) stands for the energy conservation of the direct electron at tunneling ionization. Equations (10) and (11) indicate the energy conservation of the rescattering electron at the moments of ionization and rescattering, respectively. Equation (12) represents the return condition of the rescattering electron. Note that the energy conservation of the rescattering electron at the instant of rescattering [see Eq. (11)] is the same as that of atom [42], while in Eq. (12), two additional terms of x_0 and y_0 are introduced. This is because the EWP can be released from the molecule with an initial position of \mathbf{R} , and then it is driven back to the parent ion undergoing a rescattering with the molecular center. The tunneled EWP spreads from the initial position to the molecule, and the potential energy term of $-x_0 E(t_0^r)$ is thus induced in Eqs. (9) and (10).

It should be mentioned that the transition amplitudes of the direct and near-forward rescattering electrons in Eq. (4) affect the contrast of holographic interference fringes, and their phase difference $\Delta\Phi$ decides the position of interference fringes that we are interested in. Thus for simplicity, we omit the transition amplitudes in the paper, and consider the phase difference $\Delta\Phi$ only.

III. RESULTS AND DISCUSSION

In Figs. 1(a) to 1(c), we show PEMDs for strong-field tunneling ionization of N_2 at three different alignments. The laser field is linearly polarized along the \hat{x} axis, and the molecule is aligned in the laser polarization direction with the angles of $\theta = 0, \pi/4$, and $\pi/2$, respectively. The intensity of the laser field is 2.5×10^{14} W/cm² and the wavelength is 1000 nm. At first glance, there are three types of interference fringes that can be clearly observed from these PEMDs. The first one presented as a ring-like structure centered around zero momentum is the intercycle interference, known as the above-threshold ionization peaks. The nearly vertical one, most visible on the p_x axis, originates from the interference of the direct electrons tunneling ionized during the adjacent quarter cycles of the laser pulse [64–66]. In PEMDs, these two types of interference fringes are intertwined, and in experiments, they are usually invisible due to the laser focal volume effect. The other nearly horizontal fringes are referred as holographic interference, which stems from the interference of the electrons reaching to the detector directly after tunneling and those undergoing a near-forward rescattering with the parent ion [30]. This interference structure is observed in a broad range of experiments, and it is the

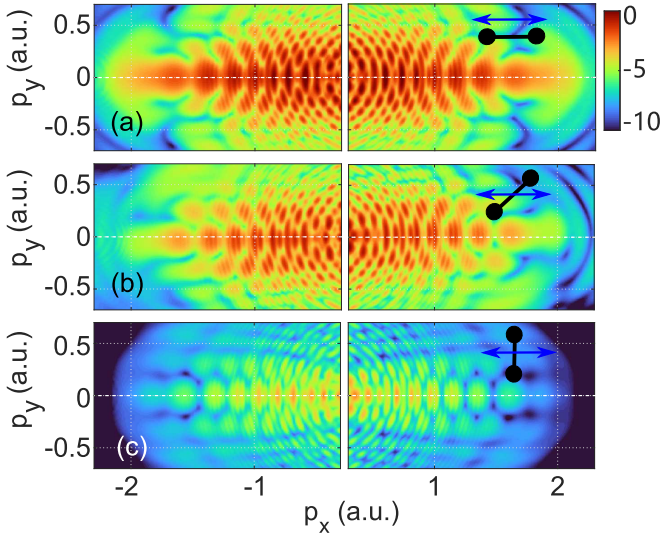


FIG. 1. (a)–(c) PEMDs for strong-field tunneling ionization of N_2 where the molecule is aligned with the angles of $\theta = 0, \pi/4,$ and $\pi/2$ in the polarization direction of the linear laser pulse, respectively. The intensity of the laser field is $2.5 \times 10^{14} \text{ W/cm}^2$ and the wavelength is 1000 nm. The colorbars of (a)–(c) are logarithm scaled.

most pronounced interference structure in the PEMDs for the near-infrared and midinfrared laser pulses [46,67]. Here, we focus on this holographic structure.

A closer inspection shows that there is a visible difference between these holographic patterns in Figs. 1(a) to 1(c). In Figs. 1(a) and 1(c), the holographic pattern is exactly symmetric about the p_x axis and the interference fringes always maximize at $p_y = 0$. While, in Fig. 1(b), the holographic structure is asymmetric, and it shows a remarkable shift along the direction perpendicular to the laser polarization. More obviously, the shift of the holographic pattern can be seen from Figs. 2(a) and 2(b), where we washed out the vertical interference fringes by averaging the raw PEMDs over p_x with a window function [39], and several cuts of the obtained

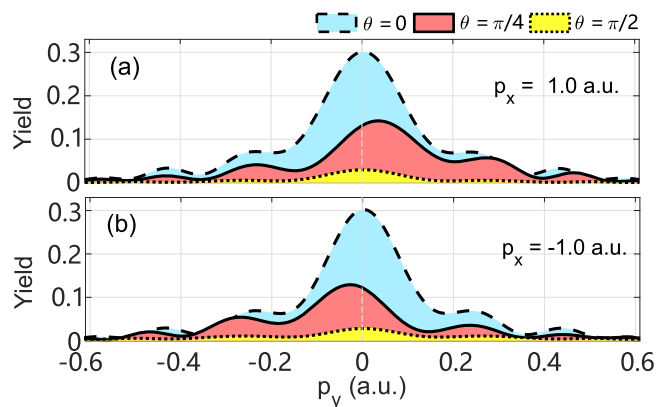


FIG. 2. (a) The averaged PEMDs at the cut of $p_x = 1.0 \text{ a.u.}$ (b) The same as (a), but for the cut of $p_x = -1.0 \text{ a.u.}$ In (a) and (b), the dashed, solid, and dotted curves represent the results of the molecule with the alignment angles $\theta = 0, \pi/4,$ and $\pi/2,$ respectively.

PEMDs for three alignments are presented. It is shown that, for the alignment of $\theta = \pi/4$, the interference minima or maxima shift left at $p_x = -1.0 \text{ a.u.}$, and they shift right at 1.0 a.u. . We should mention that this phenomenon is in good agreement with the recent experiments [27,31], where the shift of the holographic interference for the aligned molecule was clearly observed. In previous studies, it was reported that the shift of holographic interference is related to the phase structure of the tunneling ionized EWP [28]. Here, we demonstrate that the holographic interference shift directly corresponds to the initial spatial lateral coordinates of the EWP emitted from the molecule in tunneling ionization. By analyzing the shift of holographic interference fringes, the transverse emission displacement of the tunneling EWP can be retrieved accurately. In our study, the hologram is centrosymmetric about $(p_x = 0, p_y = 0)$, and thus we take the interference fringes in the momentum region of $p_x < 0$ as an example for analysis in the followings.

In strong-field tunneling ionization, the electron is usually emitted from the atom with zero initial displacement in the direction perpendicular to the laser polarization. While for the molecule, there is a nonzero initial transverse displacement of the tunneling EWP, due to the anisotropic molecular structure. This transverse displacement relates to the electronic structure and the alignment of the molecule. Therefore, to survey the holographic interference for strong-field tunneling ionization of N_2 , we monitor the time evolution of the electron density distribution for the aligned molecule. Figure 3(a) shows the linearly polarized laser field that we utilize, and Fig. 3(b) shows the electron density distribution of the aligned N_2 at the instant near the peak of the laser field. For a better view, several cuts of the electron density distribution at $x = 12 \text{ a.u.}$ and 14 a.u. are illustrated in Fig. 3(c), where the solid and dotted blue curves indicate the amplitude of the electron wave function and the solid orange curves indicate its phase. It is shown that for both of the parallel ($\theta = 0$) and perpendicular ($\theta = \pi/2$) alignments, the electron wave function is exactly symmetric about the \hat{x} axis and it maximizes at $y = 0$. While for the alignment of $\theta = \pi/4$, the wave function maximizes at $y = 1.6 \text{ a.u.}$ We should mention that the longitudinal emission displacement of the EWP estimated by $-I_p/E(t)$ is about 7–12 a.u. for our laser parameters. Thus, the result in Fig. 3(b) presents a picture about the transverse electron density distribution of the aligned N_2 immediately after ionization, where the location of the maximum determines the transverse launching displacement of the tunneling EWP [68]. With this picture in mind, next we reveal the origin of the holographic interference shift in PEMDs for the aligned molecule in tunneling ionization.

Figure 4(a) illustrates the schematic diagram of the electron trajectories in tunneling ionization of the molecule. For aligned N_2 , when the ionization occurs at the falling edge of the laser field, the electrons are emitted from the parent ion with a certain transverse displacement y_0 illustrated in Fig. 3(c). Driven by the oscillating electric field of the laser pulse, some of the released electrons reach to the detector directly after tunneling, while the other electrons can return back undergoing a near-forward rescattering with the molecular center. Due to the coherent nature of tunneling, these two types of electrons interfere with each other, resulting in

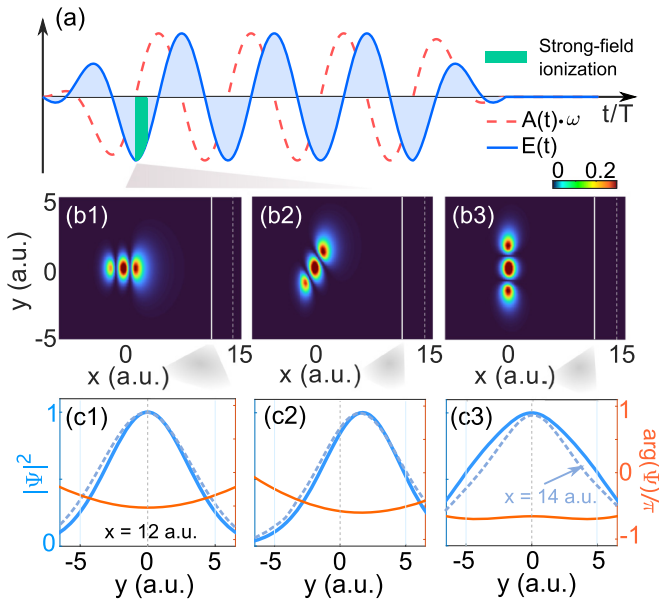


FIG. 3. (a) The electric field of the linear laser pulse (solid red curve) and its vector potential (dashed red curve). (b) Electron density distribution of N_2 in coordinate space for the instant near the laser field peak. In (b1)–(b3), the molecule is aligned in the laser polarization direction with the angles of $\theta = 0, \pi/4$, and $\pi/2$, respectively. (c) The electron density distribution of the aligned molecule at the cuts of $x = 12$ a.u. and 14 a.u. indicated by the lines in (b). The amplitudes are shown by solid and dashed blue curves, and the phases for the cut of $x = 12$ a.u. are presented by the solid orange curves. Note that two cuts of the electron density distribution amplitude are normalized such that the maximum is unity for a better view.

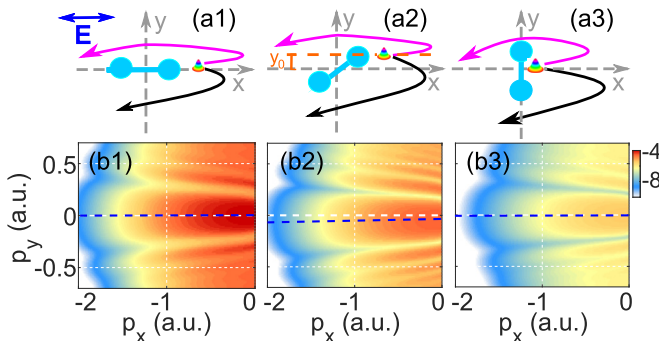


FIG. 4. (a) Sample motion trajectories of the direct and near-forward rescattering electrons. Tunneling ionization of a molecule generates an EWP. When the ionization occurs at the instant near the peak of the laser pulse, the EWP is launched from the molecule with an initial transverse displacement of y_0 (the dashed orange line) depending on the molecular alignment. The tunneled EWP subsequently spreads in the laser field, part of which reaches to the detector directly after tunneling, while the others may be driven back undergoing a near-forward rescattering with the molecular geometric center. (b) The holographic interference between the direct and near-forward rescattering EWPs, in which the initial transverse displacement y_0 of the tunneled EWP is decoded, resulting the shift of interference fringes shown by the dashed blue line in (b2). In (b1)–(b3), the results of N_2 with alignment angles of $\theta = 0, \pi/4$, and $\pi/2$ are obtained from Eq. (6), where the color coding is on a logarithmic scale.

the holographic pattern in PEMDs. With the QO model, the holographic pattern could be simulated by Eq. (6). The obtained results for tunneling ionization of N_2 are demonstrated in Figs. 4(b1) to 4(b3), where the molecule is aligned in the polarization direction of the laser field with the angles of $\theta = 0, \pi/4$, and $\pi/2$, respectively. It is shown that for both of the parallel and perpendicular alignments, the zeroth maximum of the holographic interference is located at $p_y = 0$, and for the alignment of $\theta = \pi/4$, the zeroth maximum of the interference is shifted towards the $-p_y$ direction. This result agrees well with the TDSE results displayed in Figs. 1(a) to 1(c), which implies that the shift of the holographic pattern in PEMDs is caused by the nonzero transverse emission position of the tunneling EWP.

Quantitatively, to gain the exact correspondence between the holographic interference shift and the transverse emission position of the tunneling EWP, we examine the QO model. In the QO analysis (as demonstrated in Sec. II B), the holographic structure in PEMDs is described by the phase difference between the near-forward rescattering and direct electrons in strong-field tunneling ionization, which includes two parts shown by Eq. (5). In the pioneering work on the hologram, the effects of the Coulomb interaction on the phase difference are not taken into account. Thus, the predicted holographic interference fringes deviate from the TDSE and experimental results [30,46]. This point can be seen from Figs. 1 and 4(b), where we show the TDSE results, and the results from Eq. (5) but without α . Recently, the term of α , which accounts for the interaction between the parent ion and the rescattering electron (i.e., the phase of scattering amplitude), was reported [39]. It was pointed out that, with this term included, the holographic pattern given by Eq. (5) agrees excellently with the TDSE result. However, the calculation about α is complicated and tedious, which can impede the extraction of atomic or molecular structure and electron dynamic information from the holographic pattern. Interestingly, as addressed in the following text, this Coulomb effect does not matter for the shift of holographic interference fringes, and it can be canceled out safely in our scheme.

First, we simplify the phase difference $\Delta\Phi_F$ of Eq. (5). For the holographic interference in the PEMDs, the momentum change of the electron along the y axis during the recollision process is fundamentally important. In our linear laser field, the direct electron ionizes with an initial transverse momentum close to the final transverse momentum p_y . For the rescattering electron, it tunnels with a small initial transverse momentum k_y , and gets the final transverse momentum p_y through the recollision. With the QO concept, the direct and rescattering electrons following the different pathways to the same final momentum can induce the phase difference in the transverse momentum distribution, giving rise to the fork-like holographic interference in the PEMDs [30]. For the near-forward rescattering holographic pattern that we focus on, the interference fringes exist at the momentum region of $|p_y| < 0.3$ a.u. and $p_x \in [-1.4, -0.8]$ a.u.. In this region, the rescattering electron interacts very weakly with the target [32,40,42]. In the direction parallel to the laser polarization, the momentum of electron does not even change significantly during the “soft recollision” process, and thus it allows for the assumption of $p_x \doteq k_x$. With the result, it is then obtained that

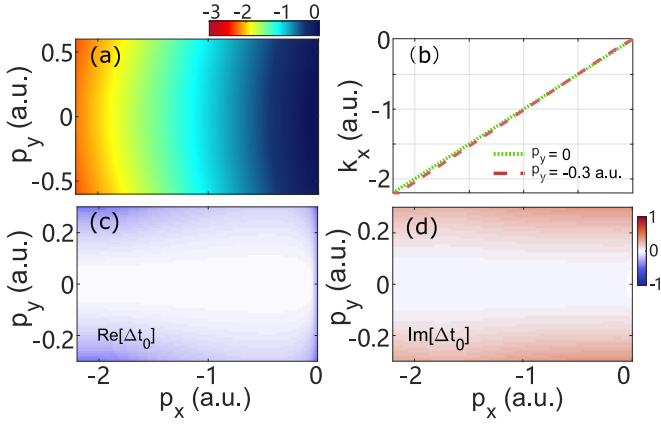


FIG. 5. (a) The parallel component of the intermediate canonical momentum k_x for $p_x \in [-2, 0]$ a.u. and $p_y \in [-0.6, 0.6]$ a.u.. (b) k_x at two cuts of $p_y = 0$ (dotted curve) and -0.3 a.u. (dashed curve). (c,d) The real and imaginary parts of the ionization time difference $\Delta t_0 = t_0^d - t_0^r$ between the direct and near-forward rescattering electrons, respectively.

the ionization times of the direct and rescattering electrons are approximately equal through Eqs. (9) and (10), i.e.,

$$t_0^d \doteq t_0^r. \quad (13)$$

Quantitatively, k_x of the rescattering electron obtained from the saddle-point equations and two cuts of k_x at $p_y = -0.3$ a.u. and 0 are displayed in Figs. 5(a) and 5(b), respectively. The differences in the real and imaginary parts of the ionization time are separately displayed in Figs. 5(c) and 5(d). It is shown that for the momentum range of $|p_y| < 0.3$ a.u., k_x is close to p_x indeed, and the time differences are well below 0.3 a.u.. This indicates that the approximations in Eq. (13) are reasonable. In the following, we will omit the superscript in t_0 .

In QO analysis, the phase difference $\Delta\Phi_F$ can be divided into two parts of $\Delta\Phi_{F_x}$ and $\Delta\Phi_{F_y}$, as shown in Eqs. (7) and (8). For the near-forward rescattering, it can be easily proved that the parallel momentum of $\Delta\Phi_{F_x}$ is approximately canceled by

$$\begin{aligned} \Delta\Phi_{F_x} &\doteq \left(\frac{p_x^2}{2} - \frac{k_x^2}{2}\right)(t_r - t_0) + (p_x - k_x) \int_{t_0}^{t_r} A(t) dt \\ &= \left(\frac{p_x^2}{2} - \frac{k_x^2}{2}\right)(t_r - t_0) + (p_x - k_x)[x_0 - k_x(t_r - t_0)] \\ &\doteq \left(\frac{p_x^2}{2} + \frac{k_x^2}{2}\right)(t_r - t_0) - p_x k_x(t_r - t_0) \\ &= \frac{1}{2}(t_r - t_0)(p_x - k_x)^2 \\ &\doteq 0, \end{aligned} \quad (14)$$

and the transverse momentum of $\Delta\Phi_{F_y}$ is simplified by

$$\begin{aligned} \Delta\Phi_{F_y} &\doteq \left(\frac{p_y^2}{2} - \frac{k_y^2}{2}\right)(t_r - t_0) + (k_y - p_y)y_0 \\ &= \left(\frac{p_y^2}{2} - \frac{k_y^2}{2}\right)(t_r - t_0) + k_y(k_y - p_y)(t_r - t_0) \end{aligned}$$

$$\begin{aligned} &= \left(\frac{p_y^2}{2} + \frac{k_y^2}{2}\right)(t_r - t_0) - k_y p_y(t_r - t_0) \\ &= \frac{1}{2}(t_r - t_0)(p_y - k_y)^2. \end{aligned} \quad (15)$$

Here, Eq. (13) is involved in Eqs. (14) and (15). Additionally, for both Eqs. (14) and (15), the saddle-point equation of Eq. (12) is employed, i.e.,

$$\begin{aligned} k_x &= [x_0 - \int_{t_0}^{t_r} A(t) dt] / (t_r - t_0), \\ k_y &= y_0 / (t_r - t_0). \end{aligned} \quad (16)$$

With the obtained Eqs. (14) and (15), the phase difference $\Delta\Phi$ of the direct and near-forward rescattering electrons in tunneling ionization is eventually rewritten in a very simple form

$$\begin{aligned} \Delta\Phi &= \Delta\Phi_F + \alpha \\ &= \frac{1}{2}(t_r - t_0)(p_y - k_y)^2 + \alpha. \end{aligned} \quad (17)$$

Through Eq. (17), the transverse momentum p_y of the holographic interference minima or maxima [where $\Delta\Phi = n\pi$ ($n = 0, 1, 2$)] is straightforwardly given by

$$p_y = \pm \sqrt{\frac{2(n\pi - \alpha)}{t_r - t_0}} + k_y. \quad (18)$$

Here, k_y indicates the transverse component of the intermediate canonical momentum for the near-forward rescattering electron, and it corresponds to the transverse emission position of the tunneling EWP through Eq. (16). The shift of the holographic interference for the molecule with the alignment angle of θ relative to that with 0 is subsequently obtained by

$$\begin{aligned} \Delta p_y &= p_y(\theta) - p_y(0) \\ &= \pm \sqrt{\frac{2(n\pi - \alpha)}{t_r - t_0}} + k_y(\theta) \mp \sqrt{\frac{2(n\pi - \alpha)}{t_r - t_0}} - k_y(0). \end{aligned} \quad (19)$$

In Eq. (19), α is the phase induced by the Coulomb interaction between the parent ion and the rescattering electron. For p_y close to 0 , it is almost unchanged with θ [39,69]. When the molecule is aligned to the linearly polarized laser field with $\theta = 0$, the EWP is driven out of the molecule along the laser polarization direction with zero transverse displacement. Thus, we have $k_y(0) = 0$. Equation (19) is rewritten as

$$\Delta p_y = k_y(\theta) = y_0 / (t_r - t_0). \quad (20)$$

Equation (20) shows that the shift of holographic interference is induced by the transverse emission position y_0 of the tunneling EWP, and it is related to the parallel momentum p_x through the time difference between the recollision and ionization of the near-forward rescattering electron. The Coulomb interaction between the parent ion and the rescattering electron influences the position of the interference fringes, but it does not affect the shift of the interference fringes. Therefore, by analyzing the shift of holographic interference for the molecule with the alignment angle of θ relative to that with 0 , the transverse emission position y_0 for the tunneling

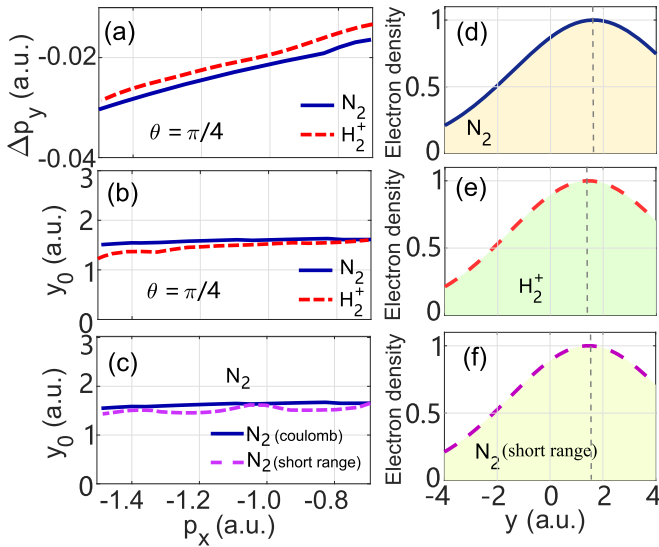


FIG. 6. (a) The shift Δp_y for the zeroth maximum of the holographic interference. The solid blue and dashed red curves represent the results of N_2 and H_2^+ aligned with the angle of $\theta = \pi/4$ in the laser polarization direction, respectively. (b) The transverse emission position y_0 of the tunneled EWP retrieved from (a). (c) The same as (b), but the dashed curve represents the result of the molecule with the short-range potential. (d) The transverse electron density distribution of N_2 as a function of the coordinate x for the instant near the laser pulse peak. The result is normalized such that the maximum is unity. (e) The same as (d), but for H_2^+ . (f) The same as (d), but for the molecule with the short-range potential.

EWP is accurately retrieved. Moreover, Eq. (20) indicates that we can focus on the zeroth maximum of the holographic interference, which is clearly visible experimentally. For the molecule with the alignment angle of $\theta = 0$, the zeroth maximum of the holographic interference is always located at $p_y = 0$. In Eq. (20) the recollision and ionization times of the electron can be obtained from Ref. [42], in which the results are consistent with that from the QO model. Therefore, through Eq. (20) the transverse emission position of the tunneling EWP is directly determined by the zeroth maximum shift of the holographic interference in PEMDs. This is a key point of our scheme. It should be mentioned that y_0 represents the transverse displacement of the EWP emitted from the molecule with respect to the rescattering point. For the near-forward rescattering, the corresponding impact parameter is larger, and thus the rescattering EWP does not feel the asymmetric potential of the aligned molecule. At a large distance from the molecule, the molecular potential is nearly isotropic. Therefore, the recollision occurs almost at the molecular center.

To demonstrate the retrieval of y_0 for strong-field tunneling ionization of N_2 , we trace the zeroth maximum of the holographic interference in the PEMD for each p_x . The obtained Δp_y for N_2 aligned with the angle of $\theta = \pi/4$ in the linearly polarized laser field is presented in Fig. 6(a). It is clear that $|\Delta p_y|$ shown by the solid curve gradually increases with the parallel momentum $|p_x|$. With this dependence, the transverse emission position of y_0 for the tunneling EWP is

extracted through Eq. (20). The obtained results are presented in Fig. 6(b), where y_0 is nearly independent on the final electron momentum p_x . By averaging the data for p_x varying from -1.5 a.u. to -0.7 a.u., the transverse emission position of the tunneling EWP is eventually determined by $y_0 = 1.58$ a.u. To check the accuracy of the result, we refer to the electron density of N_2 . For the laser parameters in our calculation, the longitude tunneling exit is approximately 7–12 a.u.. Thus, we trace the time evolution of the electron density and integrate it from $x = 12$ a.u. to the boundary at each time step during the time propagation. The transverse electron density distribution for the instant near the peak of the laser field is obtained, as shown in Fig. 6(d). It is clear that the density distribution is maximized at $y = 1.6$ a.u.. The location of the maximum electron density distribution shows that the tunneling EWP is emitted from the molecule with an initial displacement in the direction perpendicular to the tunnel [68]. The retrieved y_0 in Fig. 6(b) agrees well with the result. It indicates that the transverse emission displacement of the tunneling EWP is accurately retrieved with our scheme.

To check the validity of our scheme, we apply our scheme to strong-field tunneling ionization of H_2^+ as well. In Figs. 6(a) and 6(b), the obtained Δp_y and y_0 for the zeroth maximum of the holographic interference are shown by the dashed curves. In Fig. 6(e), the transverse electron density distribution for H_2^+ is displayed. It is shown that the density distribution maximizes at $y = 1.34$ a.u. and the average of y_0 for different p_x is about 1.4 a.u.. The good agreement between these two results indicates that our retrieval scheme is valid. Further, we illustrate our scheme for the short-range potential. In the short-range potential, the screening is introduced by multiplying the molecular potential by an isotropic cutoff term $e^{-(r-r_0)}$ for the radial distance r larger than $r_0 = 3.5$ a.u., where r_0 represents the spatial extent of the molecule [70]. The screening procedure was established in the previous study of Ref. [10] and it can cancel the influence of the long-range potential on electron scattering. Here, for the screened molecule, the obtained y_0 and transverse electron density distribution are presented in Figs. 6(c) and 6(f), respectively. For comparison, the results of N_2 with the Coulomb potential are also presented in Fig. 6(c). It is shown that for the short-range potentials, $y_0 = 1.57$ a.u., which agrees well with that of the Coulomb potential, and it is consistent with the transverse displacement of the maximum electron density distribution in Fig. 6(f). This indicates that the Coulomb potential does not affect the shift of holographic interference fringes and it can be safely canceled in our scheme. The validation of the approximation made in Eq. (20) is thus confirmed.

Furthermore, we survey the transverse emission position of the tunneling EWP for the molecule with different alignments. The results are presented in Fig. 7, where N_2 and H_2^+ are aligned in the polarization direction of the laser field with the angles of θ ranging from 0 to $\pi/2$. The circles indicate the results exacted from the shift of holographic interference, and the bars present the data obtained from the transverse electron density distribution. It is shown that y_0 obtained from the holographic interference agrees excellently with the peak position of the transverse electron density distribution, which confirms that our retrieval scheme is accurate and effective for different molecules and alignments. Moreover, as

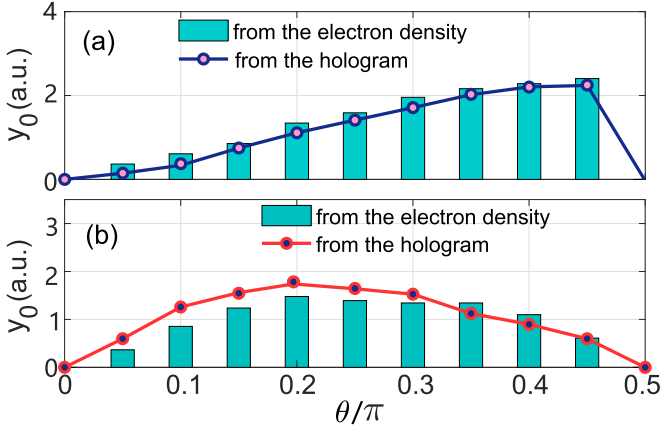


FIG. 7. (a) y_0 of the tunneled EWP for N_2 (with the internuclear distance of 2 a.u.) aligned in the laser polarization direction with θ ranging from 0 to $\pi/2$. The data of circles are exacted from the shift of the holographic interference and that of the bars are obtained from the transverse electron density distribution. (b) The same as (a), but for H_2^+ with the internuclear distance of 4 a.u.

the alignment angle increases, the transverse displacement of the electron density distribution increases first and then decreases for both of N_2 and H_2^+ . A closer inspection of Fig. 7 shows that, the dependence of y_0 on the molecular alignment is extraordinarily different for N_2 and H_2^+ . This difference may be attributed to the discrepancy of the molecular orbital. Considering the molecular orbital as linear combinations of atomic orbitals, the highest-occupied molecular orbital of H_2^+ is $1s\sigma_g$, which is contributed by the atomic s orbitals only. For N_2 , the highest-occupied molecular orbital is also σ_g , while the atomic p orbital has significant contributions to it [47]. The probability distribution of the p orbital is very different from the s orbital, which leads to the discrepancy in Figs. 7(a) and 7(b). Thus, the dependence of y_0 on the molecular alignment indicates that the shift of the holographic fringes encodes the information of the electronic structure of molecules, not the internuclear distance. The dependence difference between N_2 and H_2^+ shows that this electronic structure sensitively depends on the molecular orbital and alignment.

Last but not least, we retrieve the transverse emission positions of the EWP for various laser intensities and wavelengths. The obtained results for N_2 with the alignment angle of $\theta = \pi/4$ are presented in Fig. 8, where Fig. 8(a) shows the data for different laser intensities of $3.0 \times 10^{12} \text{ W/cm}^2$ (dotted curve), $2.5 \times 10^{12} \text{ W/cm}^2$ (solid curve), and $2.0 \times 10^{12} \text{ W/cm}^2$ (dashed curve). Figure 8(c) presents the results for different wavelengths of 1200 nm (dotted curve), 1000 nm (solid curve), and 800 nm (dashed curve). The corresponding transverse electron density distributions of molecules are shown in Figs. 8(b) and 8(d). It is clear that the transverse emission position of y_0 is almost unchanged with our laser parameters. At all laser intensities and wavelengths, it is about 1.58 a.u. and the maximum of the transverse electron density distribution is well located at $y = 1.6$ a.u. The good agreement between these two results confirms that our scheme is stable for different laser parameters.

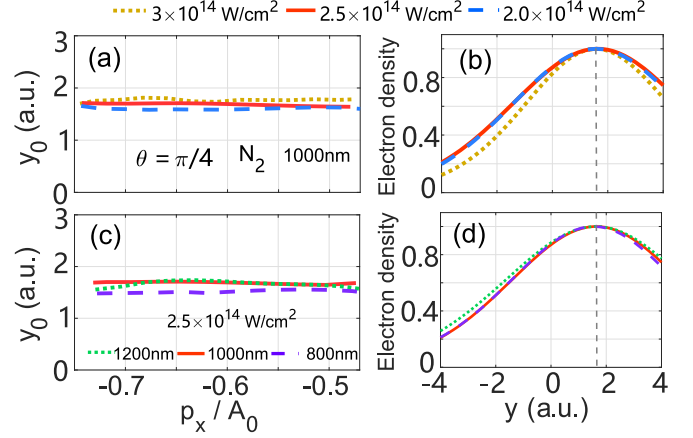


FIG. 8. (a) The retrieved y_0 as functions of p_x for different laser intensities of $3.0 \times 10^{12} \text{ W/cm}^2$ (dotted curve), $2.5 \times 10^{12} \text{ W/cm}^2$ (solid curve), and $2.0 \times 10^{12} \text{ W/cm}^2$ (dashed curve). The laser wavelength is fixed at 1000 nm. (b) The transverse electron density distribution of N_2 at three different laser intensities. (c) The same as (a), but for the laser field with the fixed intensity of $2.5 \times 10^{12} \text{ W/cm}^2$ and various wavelengths of 1200 nm (dotted curve), 1000 nm (solid curve), and 800 nm (dashed curve). (d) The same as (b), but for different wavelengths. In the calculation, N_2 is aligned in the laser polarization direction with the angle of $\theta = \pi/4$. In (a) and (c), p_x is scaled by the amplitude of the vector potential $A_0 = E_0/\omega$.

In the practical application, the holographic interference in PEMDs should be observable and measurable. In experiments, the observation of the hologram requires the ponderomotive energy of $U_p = E_0^2/4\omega^2$ is substantially larger than the photon energy [67]. For the well-known tunneling regime [Keldysh parameter $\gamma = \sqrt{I_p/(2U_p)} < 1$], the holographic interference is clearly visible, and for the multiphoton regime ($\gamma > 1$), the signature of the hologram could be observed. Therefore, our scheme is applicable for the tunneling regime. In addition, Eq. (20) shows that the shift of the holographic interference is related to the time difference between the recollision and ionization of the near-forward rescattering electron. The time difference of $t_r - t_0$ is insensitive to the laser intensity, while it depends on the laser wavelength [46]. This means that the shift of the holographic interference can vary with the laser wavelength, as shown in Fig. 9, where we present Δp_y as a function of the laser wavelength for $p_x = -0.7A_0$. The half width of the zeroth

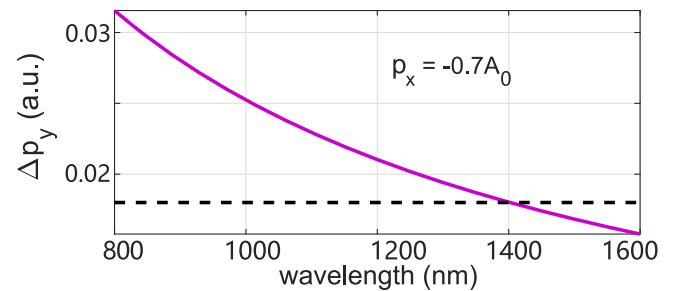


FIG. 9. For the parallel momentum of $p_x = -0.7A_0$, Δp_y indicated by the solid curve gradually varying with the laser wavelength. The dashed line represents the cut of $\Delta p_y = 0.018$ a.u..

maximum of the holographic interference is of about 0.18 a.u.. Assuming that a shift of 10% of this width could be experimentally observed. We can estimate that the laser wavelength should be smaller than 1400 nm, so that the transverse emission position of $y_0 = 1.6$ a.u. can be measured in experiments.

The principle of our scheme is that the transverse emission position of the tunneled EWP is mapped onto the phase of the transverse momentum amplitude in strong-field tunneling ionization, and it is manifested as the shift of the holographic interference in PEMDs. By examining the shift of interference fringes, the transverse emission position of the tunnel-ionized EWP can be retrieved without other reconstruction procedures and information about the target. This principle is universal for different targets. Recently, it was reported that the hologram in PEMDs for molecules can be clearly observed in experiments [27,32,71]. Thus, our study provides a general and efficient approach for direct observation of the transverse emission position of the EWP in molecules. More interestingly, the retrieved transverse displacement of the tunneling EWP is directly related to the electron density distribution in molecules. Strong-field photoelectron holography possesses particularly high time resolution [30]. In a previous study, it was demonstrated that by mapping the parallel momentum to the ionization time and treating this map as the time axis, the attosecond resolution can be achieved [39]. Based on this concept, when the ultrafast electron dynamics such as charge migration occurs in molecules with the timescale of femtosecond to attosecond, the motion of the electron could be monitored with our method. In a previous study, a proof-of-principle study of this aspect was performed [40]. Thus, our study will encourage one applying the strong-field photoelectron holography to investigate ultrafast dynamics in more complex molecules.

IV. SUMMARY

In conclusion, by solving the time-dependent Schrödinger equation in the linearly polarized laser field, we investigate

the holographic interference in PEMDs for strong-field tunneling ionization of molecules. It is shown that, when the molecule is aligned in the polarization direction of the laser field with a nonzero angle, the holographic interference in PEMDs presents a distinct shift. With the QO model, we demonstrate that the holographic interference shift is caused by the nonzero transverse displacement of the EWP emitted from the molecule, and there is an exact correspondence. By tracing the correspondence and examining the shift of the holographic interference near the field-polarization axis, the transverse emission position of the tunneling EWP is directly visualized. In intense laser atoms or molecules interactions, the Coulomb effect is a tough problem and it complicates the information retrieval from the PEMDs. Here, by performing our scheme for both of the molecules with short-range and Coulomb potentials, we demonstrate that it does not affect our scheme and can be safely canceled. Additionally, the validity and accuracy of the scheme are confirmed by applying it to different molecules, alignments, and laser parameters. Our study demonstrates a general and efficient approach for direct observation of the transverse emission position of the EWP in molecules. The obtained transverse displacement is directly related to the electron density distribution, and it depends on the molecular orbital and alignment. Thus, this study provides another insight into probing the electronic structure of molecules.

ACKNOWLEDGMENTS

J.T. gratefully acknowledges Prof. Yueming Zhou from Huazhong University of Science and Technology for his helpful discussion and suggestion. This work is supported by the starting funding of Suzhou University of Science and Technology with Grant No. 332114702, Jiangsu Key Disciplines of the Fourteenth Five-Year Plan with Grant No. 2021135, Natural Science Foundation of Jiangsu Province (Grant No. BK20220633), and National Natural Science Foundation of China (Grant No. 12204341).

-
- [1] F. Krausz and M. Ivanov, Attosecond physics, *Rev. Mod. Phys.* **81**, 163 (2009).
- [2] W. Becker, F. Grasbon, R. Kopold, D. B. Milošević, G. G. Paulus, and H. Walther, Above-threshold ionization: From classical features to quantum effect, *Adv. At. Mol. Opt. Phys.* **48**, 35 (2002).
- [3] T. Weber, H. Giessen, M. Weckenbrock, G. Urbasch, A. Staudte, L. Spielberger, O. Jagutzki, V. Mergel, M. Vollmer, and R. Dörner, Correlated electron emission in multiphoton double ionization, *Nature (London)* **405**, 658 (2000).
- [4] W. Becker, X. Liu, P. J. Ho, and J. H. Eberly, Theories of photoelectron correlation in laser-driven multiple atomic ionization, *Rev. Mod. Phys.* **84**, 1011 (2012).
- [5] Q. Ke, Y. Zhou, Y. Liao, J. Liang, Y. Zhao, and J. Tan, M. Li and P. Lu, Helicity-dependent time delays in multiphoton ionization by two-color circularly polarized laser fields, *Front. Phys.* **16**, 52503 (2021).
- [6] P. Eckle, A. N. Pfeiffer, C. Cirelli, A. Staudte, R. Dörner, H. G. Muller, M. Büttiker, and U. Keller, Attosecond ionization and tunneling delay time measurements in helium, *Science* **322**, 1525 (2008).
- [7] D. Shafir, H. Soifer, B. D. Bruner, M. Dagan, Y. Mairesse, S. Patchkovskii, M. Y. Ivanov, O. Smirnova, and N. Dudovich, Resolving the time when an electron exits a tunneling barrier, *Nature (London)* **485**, 343 (2012).
- [8] O. Pedatzur, G. Orenstein, V. Serbinenko, H. Soifer, B. D. Bruner, A. J. Uzan, D. S. Brambila, A. G. Harvey, L. Torlina, F. Morales, O. Smirnova, and N. Dudovich, Attosecond tunneling interferometry, *Nat. Phys.* **11**, 815 (2015).
- [9] J. Zhao and M. Lein, Determination of Ionization and Tunneling Times in High-Order Harmonic Generation, *Phys. Rev. Lett.* **111**, 043901 (2013).
- [10] L. Torlina, F. Morales, J. Kaushal, I. Ivanov, A. Kheifets, A. Zielinski, A. Scrinzi, H. G. Muller, S. Sukiasyan, M. Ivanov, and O. Smirnova, Interpreting attoclock measurements of tunnelling times, *Nat. Phys.* **11**, 503 (2015).

- [11] N. Camus, E. Yakaboylu, L. Fechner, M. Klaiber, M. Laux, Y. Mi, K. Z. Hatsagorsyan, T. Pfeifer, C. H. Keitel, and R. Moshhammer, Experimental Evidence for Quantum Tunneling Time, *Phys. Rev. Lett.* **119**, 023201 (2017).
- [12] U. Sainadh, H. Xu, X. Wang, A. Atia-Tul-Noor, W. Wallace, N. Douguet, A. Bray, I. Ivanov, K. Bartschat, A. Kheifets, R. Sang, and I. Litvinyuk, Attosecond angular streaking and tunnelling time in atomic hydrogen, *Nature (London)* **568**, 75 (2019).
- [13] W. Quan, V. V. Serov, M. Z. Wei, M. Zhao, Y. Zhou, Y. L. Wang, X. Y. Lai, A. S. Kheifets, and X. J. Liu, Attosecond Molecular Angular Streaking with All-Ionic Fragments Detection, *Phys. Rev. Lett.* **123**, 223204 (2019).
- [14] T. Yan, Sub-barrier Coulomb effects on the interference pattern in tunneling-ionization photoelectron spectra, *Phys. Rev. A* **86**, 053403 (2012).
- [15] M. Han, P. Ge, Y. Shao, M. Liu, Y. Deng, C. Wu, Q. Gong, and Y. Liu, Revealing the Sub-Barrier Phase using a Spatiotemporal Interferometer with Orthogonal Two-Color Laser Fields of Comparable Intensity, *Phys. Rev. Lett.* **119**, 073201 (2017).
- [16] M. Han, P. Ge, J. Wang *et al.*, Complete characterization of sub-Coulomb-barrier tunneling with phase-of-phase attoclock, *Nat. Photonics* **15**, 765 (2021).
- [17] M. Li, H. Xie, W. Cao, S. Luo, J. Tan, Y. Feng, B. Du, W. Zhang, Y. Li, Q. Zhang, P. Lan, Y. Zhou, and P. Lu, Photoelectron Holographic Interferometry to Probe the Longitudinal Momentum Offset at the Tunnel Exit, *Phys. Rev. Lett.* **122**, 183202 (2019).
- [18] P. B. Corkum, Plasma Perspective on Strong Field Multiphoton Ionization, *Phys. Rev. Lett.* **71**, 1994 (1993).
- [19] J. Liu, D. F. Ye, J. Chen, and X. Liu, Complex Dynamics of Correlated Electrons in Molecular Double Ionization by an Ultrashort Intense Laser Pulse, *Phys. Rev. Lett.* **99**, 013003 (2007).
- [20] X.-B. Bian, Y. Huismans, O. Smirnova, K. Yuan, M. J. J. Vrakking, and A. D. Bandrauk, Subcycle interference dynamics of time-resolved photoelectron holography with midinfrared laser pulses, *Phys. Rev. A* **84**, 043420 (2011).
- [21] X. Xie, S. Roither, D. Kartashov, E. Persson, D. G. Arbó, L. Zhang, S. Gräfe, M. S. Schöffler, J. Burgdörfer, A. Baltuška, and M. Kitzler, Attosecond Probe of Valence-Electron Wave Packets by Subcycle Sculpted Laser Fields, *Phys. Rev. Lett.* **108**, 193004 (2012).
- [22] D. Hickstein, P. Ranitovic, S. Witte, X. Tong, Y. Huismans, P. Arpin, X. Zhou, K. Keister, C. Hogle, B. Zhang, C. Ding, P. Johnsson, N. Tushima, M. Vrakking, M. Murnane, and H. Kapteyn, Direct Visualization of Laser-Driven Electron Multiple Scattering and Tunneling Distance in Strong-Field Ionization, *Phys. Rev. Lett.* **109**, 073004 (2012).
- [23] X. Lai, C. Wang, Y. Chen, Z. Hu, W. Quan, and X. Liu, Elliptical Polarization Favors Long Quantum Orbits in High-Order Above-Threshold Ionization of Noble Gases, *Phys. Rev. Lett.* **110**, 043002 (2013).
- [24] M. Li, J. W. Geng, H. Liu, Y. Deng, C. Wu, L. Y. Peng, Q. Gong, and Y. Liu, Classical-Quantum Correspondence for Above-Threshold Ionization, *Phys. Rev. Lett.* **112**, 113002 (2014).
- [25] J. Tan, S. Xu, X. Han, Y. Zhou, M. Li, W. Cao, Q. Zhang, and P. Lu, Resolving and weighing the quantum orbits in strong-field tunneling ionization, *Adv. Photonics* **3**, 035001 (2021).
- [26] A. N. Pfeiffer, C. Cirelli, M. Smolarski, D. Dimitrovski, M. Abu-samaha, L. B. Madsen, and U. Keller, Attoclock reveals natural coordinates of the laser-induced tunneling current flow in atoms, *Nat. Phys.* **8**, 76 (2012).
- [27] M. Meckel, A. Staudte, S. Patchkovskii, D. Villeneuve, P. Corkum, R. Dörner, and M. Spanner, Signatures of the continuum electron phase in molecular strong-field photoelectron holography, *Nat. Phys.* **10**, 594 (2014).
- [28] M. M. Liu, M. Li, C. Wu, Q. Gong, A. Staudte, and Y. Liu, Phase Structure of Strong-Field Tunneling Wave Packet from Molecules, *Phys. Rev. Lett.* **116**, 163004 (2016).
- [29] Y. Zhou, J. Tan, M. Li, and P. Lu, Probing the launching position of the electron wave packet in molecule strong-field tunneling ionization, *Sci. China Phys. Mech. Astron.* **64**, 273011 (2021).
- [30] Y. Huismans, A. Rouzée, A. Gijsbertsen, J. Jungmann, A. Smolkowska, P. Logman, F. Lépine, C. Cauchy, S. Zamith, T. Marchenko, J. Bakker, G. Berden, B. Redlich, A. van der Meer, H. Muller, W. Vermin, K. Schafer, M. Spanner, M. Ivanov, O. Smirnova, D. Bauer, S. Popruzhenko, and M. Vrakking, Time-resolved holography with photoelectrons, *Science* **331**, 61 (2011).
- [31] L. Ortmann, A. Alshafe, A. Staudte, and A. S. Landsman, Tracking the Ionization Site in Neutral Molecules, *Phys. Rev. Lett.* **127**, 213201 (2021).
- [32] W. Xie, J. Yan, M. Li, C. Cao, K. Guo, Y. Zhou, and P. Lu, Picometer-Resolved Photoemission Position within the Molecule by Strong-Field Photoelectron Holography, *Phys. Rev. Lett.* **127**, 263202 (2021).
- [33] P. A. Korneev, S. V. Popruzhenko, and S. P. Goreslavski, Interference Carpets in Above-Threshold Ionization: From the Coulomb-Free to the Coulomb-Dominated Regime, *Phys. Rev. Lett.* **108**, 223601 (2012).
- [34] X.-B. Bian and A. D. Bandrauk, Attosecond Time-Resolved Imaging of Molecular Structure by Photoelectron Holography, *Phys. Rev. Lett.* **108**, 263003 (2012).
- [35] W. Yang, H. Zhang, C. Lin, J. Xu, Z. Sheng, X. Song, S. Hu, and J. Chen, Momentum mapping of continuum-electron wavepacket interference, *Phys. Rev. A* **94**, 043419 (2016).
- [36] S. G. Walt, N. B. Ram, M. Atala, N. I. S. Shilovski, A. Conta, D. Baykusheva, M. Lein, and H. J. Wörner, Dynamics of valence-shell electrons and nuclei probed by strongfield holography and rescattering, *Nat. Commun.* **8**, 15651 (2017).
- [37] Q. Xia, J. Tao, J. Cai, L. Fu, and J. Liu, Quantum Interference of Glory Rescattering in Strong-Field Atomic Ionization, *Phys. Rev. Lett.* **121**, 143201 (2018).
- [38] J. Liang, Y. Zhou, Y. Liao, W. Jiang, M. Li, and P. Lu, Direct visualization of deforming atomic wavefunction in ultraintense high-frequency laser pulses, *Ultrafast Sci.* **2022**, 9842716 (2022).
- [39] Y. Zhou, O. I. Tolstikhin, and T. Morishita, Near-Forward Rescattering Photoelectron Holography in Strong-Field Ionization: Extraction of the Phase of the Scattering Amplitude, *Phys. Rev. Lett.* **116**, 173001 (2016).
- [40] M. He, Y. Li, Y. Zhou, M. Li, W. Cao, and P. Lu, Direct Visualization of Valence Electron Motion Using Strong-Field Photoelectron Holography, *Phys. Rev. Lett.* **120**, 133204 (2018).
- [41] G. Porat, G. Alon, S. Rozen, O. Pedatzur, M. Krüger, D. Azoury, A. Natan, G. Orenstein, B. D. Bruner, M. J. J. Vrakking, and N. Dudovich, Attosecond time-resolved photoelectron holography, *Nat. Commun.* **9**, 2805 (2018).

- [42] J. Tan, Y. Zhou, M. He, Y. Chen, Q. Ke, J. Liang, X. Zhu, M. Li, and P. Lu, Determination of the Ionization Time Using Attosecond Photoelectron Interferometry, *Phys. Rev. Lett.* **121**, 253203 (2018).
- [43] J. Tan, Y. Zhou, M. He, Q. Ke, J. Liang, Y. Li, M. Li, and P. Lu, Time-resolving tunneling ionization via strong-field photoelectron holography, *Phys. Rev. A* **99**, 033402 (2019).
- [44] C. I. Blaga, F. Catoire, P. Colosimo, G. G. Paulus, H. G. Muller, P. Agostini, and L. F. Dimauro, Strong-field photoionization revisited, *Nat. Phys.* **5**, 335 (2009).
- [45] W. Quan, Z. Lin, M. Wu, H. Kang, H. Liu, X. Liu, J. Chen, J. Liu, X. T. He, S. G. Chen, H. Xiong, L. Guo, H. Xu, Y. Fu, Y. Cheng, and Z. Z. Xu, Classical Aspects in Above-Threshold Ionization with a Midinfrared Strong Laser Field, *Phys. Rev. Lett.* **103**, 093001 (2009).
- [46] Y. Huismans, A. Gijsbertsen, A. S. Smolkowska, J. H. Jungmann, A. Rouzée, P. S. W. M. Logman, F. Lépine, C. Cauchy, S. Zamith, T. Marchenko, J. M. Bakker, G. Berden, B. Redlich, A. F. G. van der Meer, M. Yu. Ivanov, T.-M. Yan, D. Bauer, O. Smirnova, and M. J. J. Vrakking, Scaling Laws for Photoelectron Holography in the Midinfrared Wavelength Regime, *Phys. Rev. Lett.* **109**, 013002 (2012).
- [47] M. Peters, T. T. E. Charron, A. Keller, and O. Atabek, Laser-induced electron diffraction: A tool for molecular orbital imaging, *Phys. Rev. A* **85**, 053417 (2012).
- [48] M. Protopapas, C. H. Keitel, and P. L. Knight, Atomic physics with super-high intensity lasers, *Rep. Prog. Phys.* **60**, 389 (1997).
- [49] M. D. Feit, J. A. Fleck, and A. Steiger, Solution of the schrödinger equation by a spectral method, *J. Comput. Phys.* **47**, 412 (1982).
- [50] S. Chelkowski, C. Foisy, and A. D. Bandrauk, Electron-nuclear dynamics of multiphoton H_2^+ dissociative ionization intense laser fields, *Phys. Rev. A* **57**, 1176 (1998).
- [51] X. Tong, K. Hino, and N. Toshima, Phase-dependent atomic ionization in few-cycle intense laser fields, *Phys. Rev. A* **74**, 031405(R) (2006).
- [52] P. E. Cade and A. C. Wahl, Hartree-Fock-Roothaan wavefunctions for diatomic molecules: II. First-row homonuclear systems A_2 , A_2^\pm , and A_2^* , *At. Data Nucl. Data Tables* **13**, 339 (1974).
- [53] P. Salières, B. Carré, L. L. Déroff, F. Grasbon, G. G. Paulus, H. Walther, R. Kopold, W. Becker, D. B. Milošević, A. Sanpera, and M. Lewenstein, Feynman's path-integral approach for intense-laser-atom interactions, *Science* **292**, 902 (2001).
- [54] M. Ivanov, M. Spanner, and O. Smirnova, Anatomy of strong field ionization, *J. Mod. Opt.* **52**, 165 (2005).
- [55] D. B. Milošević, G. G. Paulus, D. Bauer, and W. Becker, Above-threshold ionization by few-cycle pulses, *J. Phys. B: At. Mol. Opt. Phys.* **39**, R203 (2006).
- [56] D. B. Milošević, Strong-field approximation for ionization of a diatomic molecule by a strong laser field, *Phys. Rev. A* **74**, 063404 (2006).
- [57] C. C. Chirilă and M. Lein, Strong-field approximation for harmonic generation in diatomic molecules, *Phys. Rev. A* **73**, 023410 (2006).
- [58] O. Smirnova, M. Spanner, and M. Y. Ivanov, Anatomy of strong field ionization II: To dress or not to dress, *J. Mod. Opt.* **54**, 1019 (2007).
- [59] M. Okunishi, R. Itaya, K. Shimada, G. Prümper, K. Ueda, M. Busuladžić, A. Gazibegović-Busuladžić, D. B. Milošević, and W. Becker, Two-Source Double-Slit Interference in Angle-Resolved High-Energy Above-Threshold Ionization Spectra of Diatoms, *Phys. Rev. Lett.* **103**, 043001 (2009).
- [60] A. Staudte, S. Patchkovskii, D. Pavičić, H. Akagi, O. Smirnova, D. Zeidler, M. Meckel, D. M. Villeneuve, R. Dörner, M. Y. Ivanov, and P. B. Corkum, Angular Tunneling Ionization Probability of Fixed-in-Space H_2 Molecules in Intense Laser Pulses, *Phys. Rev. Lett.* **102**, 033004 (2009).
- [61] Y. Li, Y. Zhou, M. He, M. Li, P. Lan, and P. Lu, Time-resolved internal-electron-scattering effect of H_2^+ in enhanced ionization regions, *Phys. Rev. A* **94**, 013422 (2016).
- [62] P. Li, Y. Sheu and S. Chul, Role of nuclear symmetry in below-threshold harmonic generation of molecules, *Phys. Rev. A* **101**, 011401(R) (2020).
- [63] M. Busuladžić and D. B. Milošević, Simulation of the above-threshold-ionization experiment using the molecular strong-field approximation: The choice of gauge, *Phys. Rev. A* **82**, 015401 (2010).
- [64] F. Lindner, M. G. Schätzel, H. Walther, A. Baltuška, E. Goulielmakis, F. Krausz, D. B. Milošević, D. Bauer, W. Becker, and G. G. Paulus, Attosecond Double-Slit Experiment, *Phys. Rev. Lett.* **95**, 040401 (2005).
- [65] D. G. Arbó, E. Persson, and J. Burgdörfer, Time double-slit interferences in strong-field tunneling ionization, *Phys. Rev. A* **74**, 063407 (2006).
- [66] M. Richter, M. Kunitski, M. Schöffler, T. Jahnke, L. P. H. Schmidt, M. Li, Y. Liu, and R. Dörner, Streaking Temporal Double-Slit Interference by an Orthogonal Two-Color Laser Field, *Phys. Rev. Lett.* **114**, 143001 (2015).
- [67] T. Marchenko, Y. Huismans, K. J. Schafer, and M. J. J. Vrakking, Criteria for the observation of strong-field photoelectron holography, *Phys. Rev. A* **84**, 053427 (2011).
- [68] D. Bondar and W. Liu, Shapes of leading tunnelling trajectories for single-electron molecular ionization, *J. Phys. A: Math. Theor.* **44**, 275301 (2011).
- [69] M. He, Y. Zhou, Y. Li, M. Li, and P. Lu, Revealing the target structure information encoded in strong-field photoelectron hologram, *Opt. Quant. Electron.* **49**, 232 (2017).
- [70] S. Rozen, S. Larroque, N. Dudovich, Y. Mairesse, and B. Pons, Enhanced chiral-sensitivity of Coulomb-focused electrons in strong field ionization, *J. Phys. B: At. Mol. Opt. Phys.* **54**, 184002 (2021).
- [71] J. Wiese, J. Onvlee, S. Trippel, and J. Küpper, Strong-field ionization of complex molecules, *Phys. Rev. Res.* **3**, 013089 (2021).